International Conference on Space Optics—ICSO 2012

Ajaccio, Corse

9–12 October 2012

An elegant Breadboard of the optical bench for eLISA/NGO

Luigi d'Arcio

Johanna Bogenstahl

Christian Diekmann

Ewan D. Fitzsimons

et al.

An Elegant Breadboard of the Optical Bench for eLISA/NGO

Luigi d'Arcio¶, Johanna Bogenstahl‡, Christian Diekmann‡, Ewan D. Fitzsimons†, Gerhard Heinzel‡,
Harm Hogenhuis§, Christian J. Killow†, Maike Lieser‡, Susanne Nikolov*, Michael Perreur-Lloyd†,
Joep Pijnenburg§, David I. Robertson†, Alasdair Taylor†, Michael Tröbs‡, Harry Ward†, Dennis Weise*

*Astrium GmbH - Satellites, 88039 Friedrichshafen, Germany
†University of Glasgow, Glasgow G12 8QQ, Scotland, UK
‡Albert Einstein Institute, Callinstrasse 38, 30167 Hannover, Germany
§TNO, P.O. Box 155, 2600 AD Delft, The Netherlands
¶ESA/ESTEC, Postbus 299, 2200 AG Noordwijk, The Netherlands

Abstract—The Laser Interferometer Space Antenna, as well as its reformulated European-only evolution, the New Gravitational-Wave Observatory, both employ heterodyne laser interferometry on million kilometer scale arm lengths in a triangular spacecraft formation, to observe gravitational waves at frequencies between 3×10^{-5} Hz and 1 Hz. The Optical Bench as central payload element realizes both the inter-spacecraft as well as local laser metrology with respect to inertial proof masses, and provides further functions, such as point-ahead accommodation, acquisition sensing, transmit beam conditioning, optical power monitoring, and laser redundancy switching.

These functions have been combined in a detailed design of an Optical Bench Elegant Breadboard, which is currently under assembly and integration. We present an overview of the realization and current performances of the Optical Bench subsystems, which employ ultraprecise piezo mechanism, ultrastable assembly techniques, and shot noise limited RF detection to achieve translation and tilt metrology at Picometer and Nanoradian noise levels.
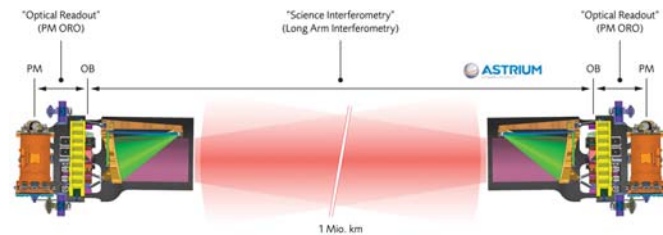
Fig. 1. Strap-Down Architecture, here illustrated for the specific case of NGO. Distance fluctuations between the two PMs of a single interferometer arm are detected by performing two local measurements and one remote measurement. PM = Proof Mass, OB = Optical Bench.

I. INTRODUCTION

THE first ideas for detection of gravitational waves by laser interferometry in space were invented more than 25 years ago, with the description of LAGOS (Laser Antenna for Gravitational-radiation Observation in Space) [1]. Since then, various mission concepts for space-borne gravitational wave observatories have been formulated and studied in partially great detail. Among the most advanced concepts is LISA (the Laser Interferometer Space Antenna), which consists of a triangular formation of 3 identical spacecraft in heliocentric orbit, mutually linked by counter-propagating laser beams over an arm length of 5 million kilometers [2], [3]. Most recently, the New Gravitational-Wave Observatory (NGO) was conceived and assessed as a possible cost-effective evolution of the LISA mission, in which only 2 interferometer arms are established between a central Mother and two Daughter spacecraft, which are separated by 1 million kilometers [4].

All mission concepts for gravitational wave detection share a number of basic characteristics, which result from the high stiffness of spacetime, and thus the need to detect extremely small fractional length changes, i.e. strain $\delta L/L$ on the scale of typically $10^{-19}/\sqrt{\text{Hz}}$ around mHz frequencies. This is achieved by realizing a very long measurement baseline L

between disturbance-free (inertial) targets, in combination with a highly sensitive measurement of pathlength fluctuations δL, which is referenced to these targets.

Both LISA and NGO share the so-called Strap-Down Architecture, which was introduced within the LISA Mission Formulation as a technical optimization to decouple the functions of local and inter-spacecraft metrology. As illustrated in Figure 1, the detection of pathlength fluctuations between the two reference targets of an individual interferometer arm is thus constructed from a total of three measurements. The Optical Bench, on which these measurement functions are integrated, consequently interfaces directly with the Gravitational Reference Sensor (GRS) on one side, and a beam expanding off-axis telescope on the other side, with an aperture diameter of 40 cm for LISA and 20 cm for NGO, respectively. These central payload elements are rigidly combined to form the so-called "Moving Optical Subassembly" (Figure 2), which is articulated to compensate for the annual variation of the inter-arm angle in the triangular spacecraft formation.

II. ELEGANT BREADBOARD FUNCTIONS AND LAYOUT

The Optical Bench Elegant Breaboard (OB EBB), which is currently under construction, has been designed and developed specifically for the mission scenario of LISA. Its full layout is illustrated in Figure 4. It includes all functions and features that would be required also for the simplified NGO concept, but in addition has a number of elements which are specific only to LISA. The functions that are foreseen on the OB EBB,
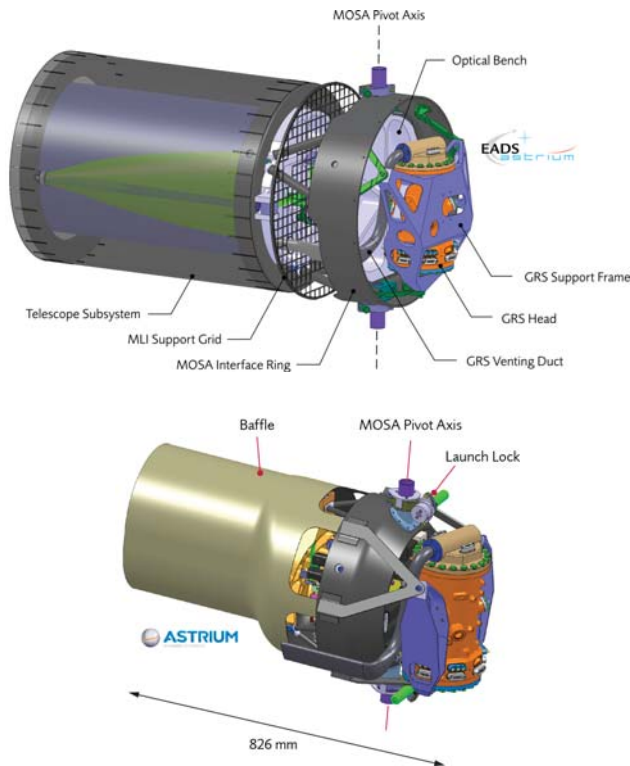
Fig. 2. Opto-mechanical design of the Moving Optical Subassemblies for LISA (top) and NGO (bottom). The GRS Head is identical in both cases, but the diameters of Optical Bench and Telescope are much smaller for the NGO design.

but which would also be presumably required for NGO, are the following:

- *Laser light delivery* for the transmit beam (TX) with implementation of switching between nominal and redundant laser source.
- A dedicated *TX Beam Clip* ensures well-defined clipping of the quasi-Gaussian profile of the TX beam to the finite aperture diameter D of the Telescope, so that the far field intensity is maximized. This is provided for $D/2w_0 = 1.12$, where w_0 is the Gaussian waist size in the aperture.
- *Backlink Fiber* interface, which connects the two Optical Benches on board each spacecraft and thus provides phase referencing between the two associated interferometer arms. The laser light obtained from the Backlink Fiber has a well-defined frequency offset with respect to the TX beam, and serves as local oscillator (LO).
- The *Reference Interferometer* establishes a phase reference between the TX and LO beams.
- The *Proof Mass Optical Readout* detects dynamical translation and tilt of the Proof Mass with respect to the interferometric reference frame establish on the Optical Bench.
- The phase of the laser light received from the remote spacecraft is observed in the *Science Interfermoter*, relative to the phase of the TX beam. By means of Differential Wavefront Sensing with Quadrant Photodiodes [5], [6], the Science Interferometer is also utilized to detect and control the spacecraft attitude relative to the

RX wavefront.
- In order to facilitate acquisition of the RX beam over an extended Field of View of about $\pm200\,\mu$rad, which is beyond the limit of contrast in the Science Interferometer, the Optical Bench includes an *Acquisition Camera*.
- A redundant *Power Monitor* photodiode is installed to detect and control optical power fluctuations of the TX beam within the measurement band.

Since the smaller arm length of NGO enables a reduction of the telescope diameter without increase of shot noise, it can also be fed with a smaller TX beam from the Optical Bench, if the telescope magnification is maintained. Therefore, a dedicated *Beam Expander* to mode-match the beam from the TX fiber injector to the telescope internal pupil diameter is required only on the LISA OB. A second important consequence of the smaller arm length for NGO is a proportional reduction of the annual point-ahead angle variation, so that an active steering of the out-of-plane point-ahead by the *Point Ahead Angle Mechanism* (PAAM) is also only necessary in
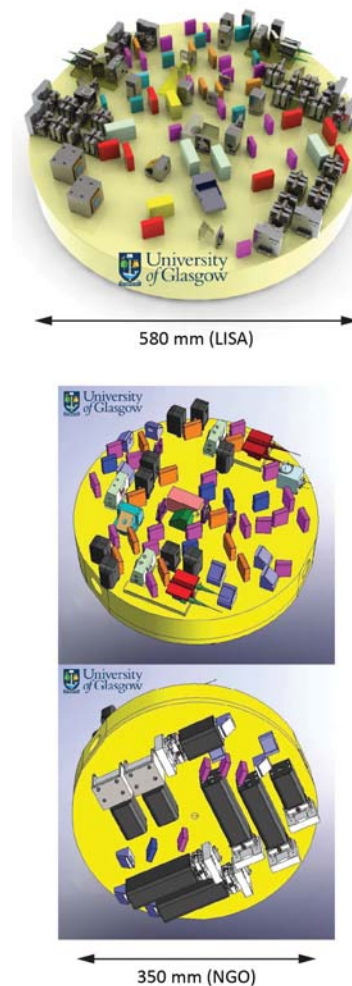

Fig. 3. Comparison of Optical Bench envelope and layout for LISA and NGO. NGO employs a double-sided layout, in which all interferometers, key interfaces, and fiber injectors are combined on one surface, and the second surface is exclusively utilized for accommodation of detector assemblies.
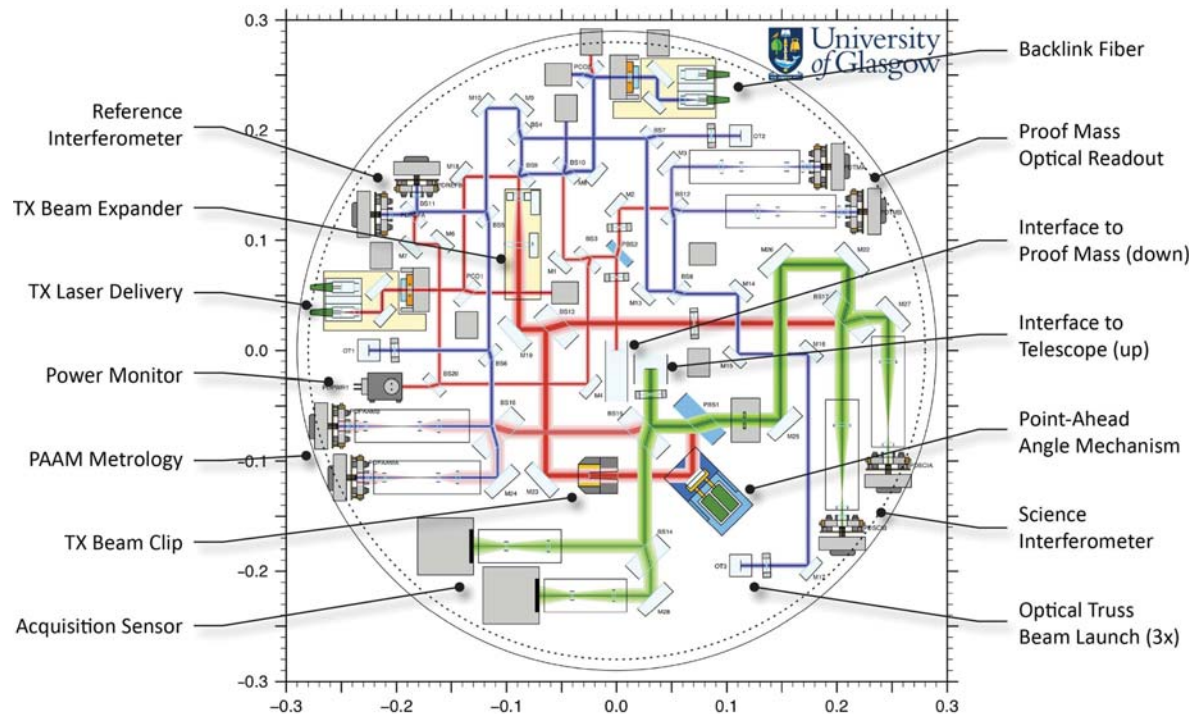
Fig. 4.   Layout of the Optical Bench EBB, which is currently under assembly and integration. The design is specific to the needs of the LISA mission scenario, but it actually includes all features also required in the case of NGO.

the specific case of the LISA mission scenario.

The Optical Bench for NGO does also not include further ancillary metrology functions, which are installed on the LISA OB to demonstrate their compatibility with the system design, as means to improve performance robustness by mitigating

 a) potential pathlength noise generated within the telescope, using an *Optical Truss* [7], and
 b) excess pathlength noise from the PAAM, using an additional interferometer for *PAAM Metrology*.

While the *PAAM Metrology* obviously is not applicable to NGO, since NGO does not utilize a PAAM, also the Optical Truss was removed from the system to enable a minimal Optical Bench diameter, and thus a significant reduction of the overall payload envelope. By additionally introducing a dual-surface Optical Bench based on a Zerodur sandwich baseplate, the Optical Bench diameter for NGO is thus reduced from 580 mm as in Figure 4 to 350 mm, as illustrated in Figure 3.

It may be concluded that the Optical Bench layout under construction here, defined by Figure 4, should represent a setup in which the metrology technology of a space-based gravitational wave observatory can be demonstrated comprehensively, independent from the exact form of final implementation.

III. Integration Technology and Optical Component Design

The optical elements utilized for beam shaping, beam steering, beam splitting, and interferometric beam combination are planned to be integrated on the Zerodur baseplate using Hydroxide Catalysis Bonding [8], a mature technology for precision assembly of quasi-monolithic interferometric

benches, which has also been applied in the construction of the engineering model and flight model Optical Benches of the LISA Technology Package on LISA Pathfinder. With the exception of the out-of-plane beam steering optics, which have a Zerodur substrate, all components are made from Fused Silica, to enable superior beam quality in transmission and reflection, and ensure compatibility with the Hydroxide Catalysis Bonding technique. The procured substrates are illustrated in Figure 5.

Since Hydroxide Catalysis Bonding does not allow for a fine-adjustment of the out-of-plane reflection angle, the tolerance on the perpendicularity between bonding surface and reflecting surface has to be well-controlled, and is typically specified to be below 2" (10 μrad). A major update to the Optical Bench design reported in [10] is that all transmissive elements have been found to require also precise parallelism between front and back surfaces, in order to avoid the generation of pathlength noise by pointing jitter within the components.

In general, it is common to specify a well-defined wedge angle between front and back surfaces of substrates for monochromatic applications, so that the risk of interference of spurious ghost beams with the main beam is minimized. However, if the pointing of the incident beam is subject to small fluctuations, these probe the varying thickness of the substrate due to the wedge, and thus cause a varying optical pathlength. The situation is schematically illustrated in Figure 6. If z_{in} is the distance from the point of rotation to the nominal point of incidence (vertex) on the beam splitter, d_{bs} is the thickness of the beam splitter, and z_{out} is the distance from the
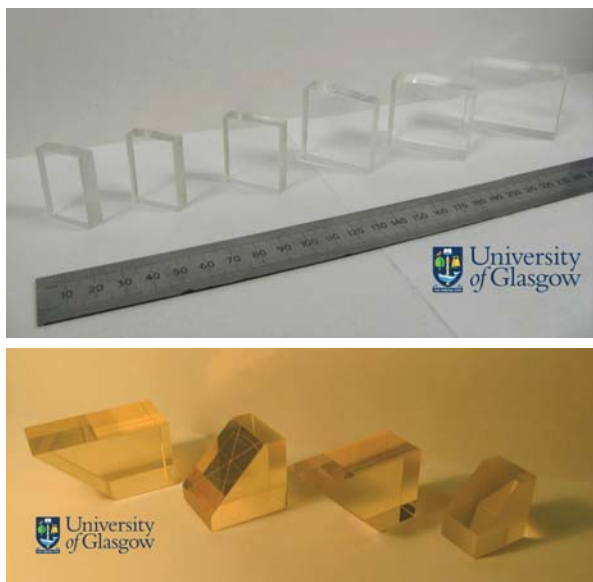
Fig. 5. Fused Silica substrates of the flat optical components (top), and Zerodur 45° mirrors for out-of-plane beam steering (bottom).

Fig. 6. Schematic illustration of the beam path through a wedged component, in the presence of pointing jitter $\delta\varphi_{in}$.

vertex to the detection plane, the optical pathlength fluctuation can be written as

$$\delta L = (c_{in}z_{in} + c_{bs}d_{bs} + c_{out}z_{out}) \cdot \delta\varphi_{in},$$

where $\delta\varphi_{in}$ is the pointing jitter of the incident beam. The coefficients c_{in}, c_{bs}, and c_{out} are complicated trigonometric functions of the nominal angle of incidence ϑ_{in}, the wedge angle ϑ_{bs} of the beam splitter, and the refractive index n of the substrate material. Assuming Fused Silica as substrate material with $n = 1.449631$ at a wavelength of 1064 nm, a nominal angle of incidence of $\vartheta_{in} = 45°$, and to first order in ϑ_{bs},

$$\delta L \approx (0 \cdot z_{in} + 0.461 \cdot d_{bs} - 0.790 \cdot z_{out}) \cdot \vartheta_{bs} \cdot \delta\varphi_{in}.$$

For the optical layout depicted in Figure 4, worst case conditions for this effect are experienced in the path of the RX beam toward the Science Interferometer, where $d_{bs} = 12$ mm, $z_{out} = 300$ mm, and the beam jitter can be as high as $\delta\varphi_{in} = 448$ nrad$/\sqrt{\text{Hz}}$ due to the residual attitude dynamics of the spacecraft. Consequently, in order to maintain the resulting pathlength noise significantly below 1 pm$/\sqrt{\text{Hz}}$ and thus negligible, the maximum allowable wedge angle of the RX/TX multiplexing beam splitter is approximately 10 μrad. Such a component would not qualify as *wedged*, so that all transmissive optical elements in the end were specified as plane-parallel flats with a parallelism of better than 2".

The metallic opto-mechanical elements to be installed on the OB EBB, such as detector mounts, mechanism mounts, beam clips, beam dumps, or waveplate supports, are designed to be integrated using an adhesive bonding technique, such as the one described in [9]. For this purpose, monolithic leaf springs in isostatic configuration are foreseen within the structure of these elements, which in most cases is made from non-magnetic Titanium, in order to minimize any residual electro-magnetic coupling to the proof mass.
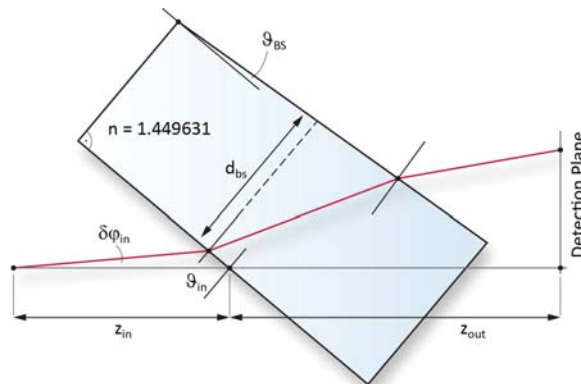
IV. FIBER INTERFACES

Laser light at 1064 nm will be delivered to the Optical Bench by singlemode, polarization maintaining fibers. These are pigtailed to so-called Fiber Switching Units (FSU), which realize the following functions:

- Appropriate collimation of the beam emerging from the fiber end, to a nominal waist radius of 1 mm.
- Implementation of redundancy switching between a nominal fiber and a redundant fiber.
- Polarization cleanup after switching.

Since contamination of an exposed fiber end was seen as a possible failure mechanism to be prevented in the redundancy scheme, free-beam switching by polarization multiplexing is implemented in the FSU design, as illustrated in Figure 7. Polarization multiplexing is chosen to minimize loss of optical power, and accomplished by using orthogonal polarizations for main and redundant beam, and switching between the two by rotation of a half waveplate after combination at a polarizing plate beam splitter.

Beam collimation and combination for the two redundant fibers is provided by Dual FIOS Assemblies, holding two identical Fiber Injector Optical Subassemblies (FIOS) for main and redundant fiber, respectively. The FIOSes are quasi-monolithic, hydroxide catalysis bonded units comprising the Fiber Mounted Assembly (FMA), which supports the fiber
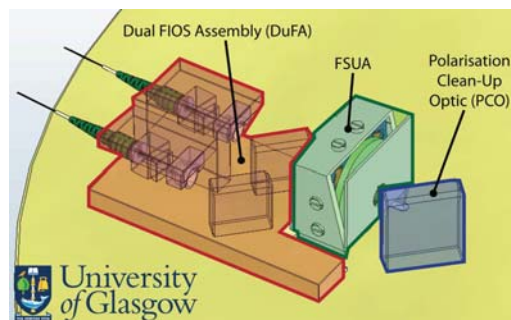

Fig. 7. Fiber Switching Unit, consisting of a Dual FIOS Assembly (DuFA), a Fiber Switching Unit Actuator (FSUA), and a polarizing beamsplitter (PCO).

Fig. 8. Left: Present FIOS design with "split spacer" to allow for a fine tuning of the optical distance between fiber end and collimating lens. Right: Elegant Breadboard of the FSU Actuator [11].

Fig. 10. Low magnification image of the polished FMA surface, clearly showing the fiber in the ferrule. The two strain relief rods and the glue layer surrounding the fiber cladding are noticably depressed.

and provides a strain relief, a Fused Silica spacer of appropriate length, and an aspheric collimating lens. The present design, depicted in Figure 8, results from an evolution of a concept realized within the LISA Technology Package for LISA Pathfinder. It implements a number of lessons learned with respect to the LTP concept and various further prototypes such as the one shown in Figure 9, which have been built to validate and consolidate the design approach:

- Due to its symmetry, the design provides optimal thermal stability for lateral alignment.
- By avoiding direct exposure of the fiber end to air or vacuum, power handling and contamination susceptibility are improved. Pending full demonstration, this design could therefore potentially facilitate the implementation of all-fiber switching for redundancy, and thus avoid the need to install switching on the Optical Bench.
- The split spacer enables a fine adjustment of the optical distance between fiber end and collimating lens, to optimize beam collimation *after* covering the bare fiber with a first bonded Fused Silica element (the "cover-slip").

Early models of fully monolithic test FIOSes experienced a strong variation in the produced beam waist, between $523\,\mu m$ and $984\,\mu m$ for a total of 5 prototypes. The inconsistency of these values with predictions based on measurements per-

formed at intermediate stages of the assembly process indicates that the final distance between fiber end and collimating lens, as well as the optical mode emerging from the fiber, were potentially not as expected. While imprinting effects on the scale of less than $20\,nm$ due to polishing of the fiber end within the FMA could be observed by phase shift interferometry with a Wyko NT1100 optical surface profiler by Veeco (Figure 10), a change of beam mode after bonding of the spacer to the FMA, and in particular the manufacturing tolerances on the curvature of the collimating lens were identified to be more likely root causes of the effect. Both are addressed by the new split spacer design of the FIOS.

Rotation of the half waveplate for selection between the two fiber ports is provided by the FSU Actuator (FSUA), depicted in Figure 8. Two elegant breadboards based on an evolution of a commercial piezo inertia actuator have been built and tested environmentally [11]. The stick-slip actuation principle enables set-and-forget operation, where power is only required during actuation. Redundancy is provided by two independent piezo stacks, which are connected to a common rotational elastic guiding.

Of crucial relevance to the performance of the entire pathlength metrology provided by the Optical Bench is the lateral pointing stability and reproducibility of the beams generated within the Fiber Switching Units. The allowable pointing variation for individual beams is on the scale of $\pm 10\,\mu rad$,
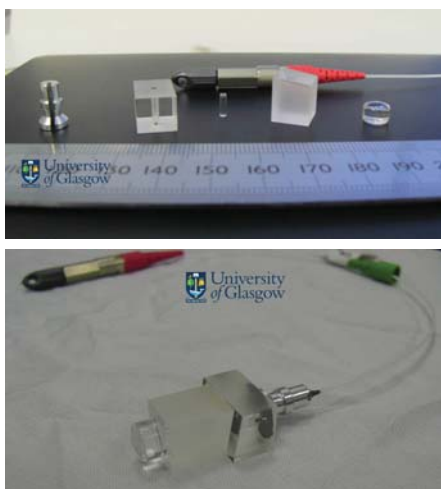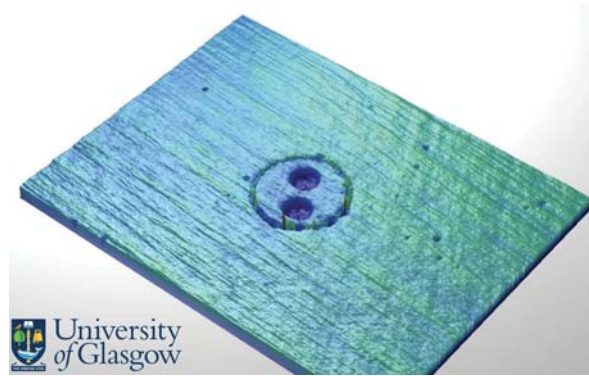

Fig. 9. The Fiber Injector Optical Subassembly is assembled from various glass elements which are joint using Hydrxoide Catalysis Bonding on all surfaces in the optical path. Various prototypes demonstrate that this can provide beams of excellent wavefront quality of $\lambda/30$ rms or lower.
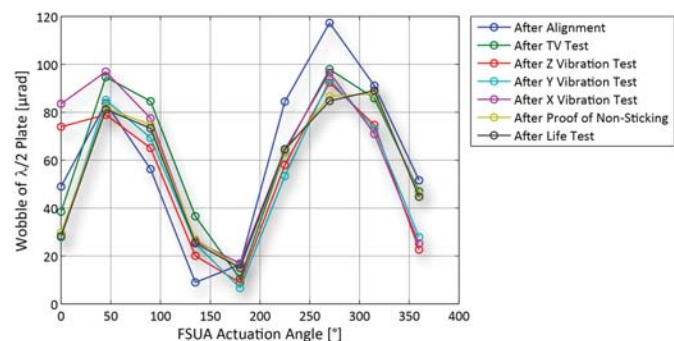

Fig. 11. Measured wobble of the waveplate within the FSUA with respect to a stable baseplate.
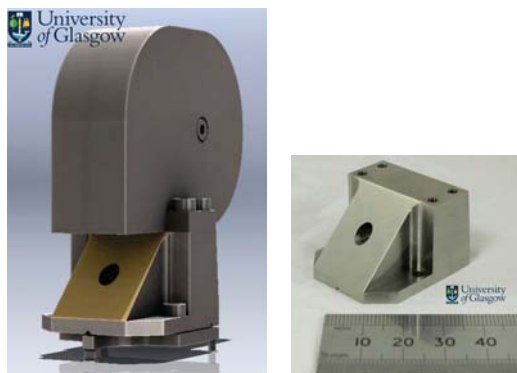
Fig. 12. Design (left) and actual reflector (right) of the TX Beam Clip. The reflection is steered to an overhead beam dump with an internal spiral minimizing any back scattering.

and $\pm 10\,\mu m$ in terms of lateral alignment offsets. The FSUA was designed to contribute a negligible fraction to this budget, so that a waveplate wobble of not more than $\pm 250\,\mu rad$ for a waveplate wedge of not more than $1\,\mu rad$ is acceptable. This requirement is met even after various steps of environmental testing, as Figure 11 demonstrates.

V. TRANSMIT BEAM CONDITIONING

The FIOSes produce an almost Gaussian beam with a nominal waist size of 1 mm, which is chosen as a compromise between good beam collimation over the dimensions of the Optical Bench, and minimal size of all optical components. This beam radius is however too small for optimal interfacing with the LISA telescope, which is designed for an internal pupil diameter of 5 mm. To maximize the on-axis far-field intensity, the optimal waist size for this physical aperture limit is given by

$$\frac{5\,mm}{2 \cdot 1.12} = 2.23\,mm.$$

The required magnification is provided on the Optical Bench by a classical afocal telescope in the TX beam path, with one concave and one convex commercial Fused Silica lens at an inter-lens spacing of approx. 41.5 mm. The lenses will be mounted from Fused Silica posts to facilitate precision control of lens centration in the out-of-plane degree of freedom.

The payload architecture actually foresees realization of the physical aperture stop of the TX beam path on the Optical Bench, to enable precise lateral alignment and well-controlled clipping of the Gaussian beam profile. In fact, optimal clipping with the above parameters leads to an optical loss of about 8.1%, or roughly 80 mW, which need to be disposed reliably – both to avoid stray light interference with other beams as well as random thermal dissipation.

This is planned to be accomplished by the TX Beam Clip design shown in Figure 12. The TX beam is incident on a gold-coated, 45 degree surface of a Titanium mount, such that its central fraction passes a tapered hole, with a diameter of 5 mm and its axis along the direction of propagation. The wings of the Gaussian beam profile are reflected up toward a special beam dump with an internal spiral that minimizes any backscattering.
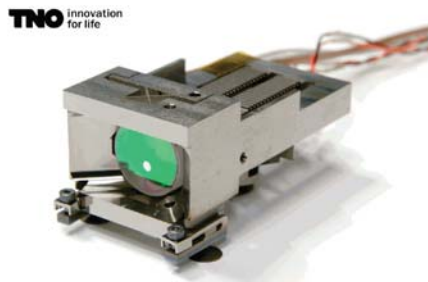

Fig. 13. Breadboard of the Point-Ahead Angle Mechanism. This design variant allows beam steering in the beam plane on the Optical Bench, i. e. the axis of rotation is perpendicular to the OB surface.

After passing the TX Beam Clip, the Point-Ahead Angle Mechanism (PAAM) provides active control of the out-of-plane Point-Ahead Angle, with respect to the axis of the RX Beam. In order to achieve an inter-spacecraft pointing range of $\pm 6\,\mu rad$, the TX beam pointing on the Optical Bench has to be controlled over a range of $\pm 580\,\mu rad$ in one degree of freedom, including margin. Since the PAAM mirror is an intrinsic element of the metrology path, it has to guarantee picometer scale pathlength stability within the measurement band. The present breadboard is illustrated in Figure 13, and has been adopted from an independent development program [11]. It utilizes piezo-driven Gimbal control of the PAAM mirror, which is supported via a monolithic Haberland hinge. Additional feet have been attached to bring the mirror center to the nominal beam height of 20 mm.

PAAM and TX Beam clip have to be installed in very close vicinity, since in combination they determine the location of the external transmit pupil. Lateral offsets of the transmit pupil from the line of sight connecting local and remote proof mass generate a lever arm which couples to spacecraft attitude noise to produce apparent pathlength measurement noise.

The optical power of the TX Beam is observed by a dedicated Power Monitor, which is used in close loop for control of residual Relative Intensity Noise (RIN) within the measurement band. As seen in Figure 14, it realizes an integrated redundancy between a nominal and a redundant photodiode by 50/50 beam splitting. A First Sensor PC50-6 photodiode is baselined for this purpose. Since the required 3 dB bandwidth of about 1 kHz is relatively low, it is not foreseen to install any
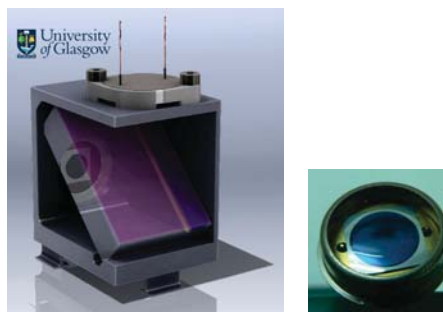

Fig. 14. Opto-mechanical design of the Power Monitor with integrated beam splitting. The selected photodiode (on the right) is a PC50-6 by First Sensor.
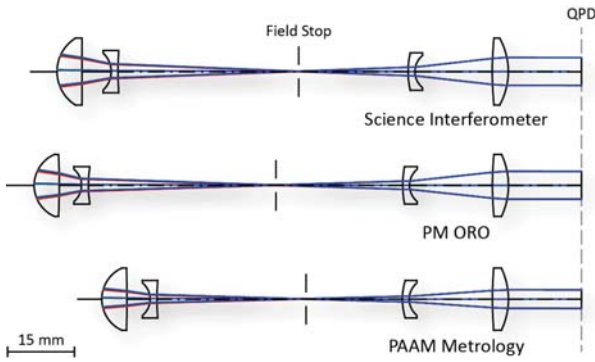
Fig. 15. Detailed optical design for the pupil relay systems foreseen for the IDAs in the Science Interferometer, the PM ORO, and the PAAM Metrology. Interferometric imaging is not foreseen for the Reference Interferometer, since both of its beams are stable.

Fig. 17. Opto-mechanical concept for accommodation of lenses and the field stop in front of the Quadrant Photodetectors. The mounts provide lockable fine-alignment capability in the lateral and out-of-plane tilt degrees of freedom.

proximity electronics directly at the photodiode on the Optical Bench, so that also power dissipation noise is of no concern here.

VI. INTERFEROMETRIC DETECTOR ASSEMBLIES

The Science Interferometer, the PM Optical Readout, and the PAAM Metrology are equipped with *Interferometric Detector Assemblies* (IDAs), which are central to the metrology concept of the OB EBB. Redundancy is provided by equipping each output of the respective recombination beam splitter with a single IDA. Each IDA consists of an interferometric imaging system followed by a Quadrant Photodiode, enabling Differential Wavefront Sensing.

The imaging systems are designed to provide optimal beam compression for a smooth wavefront and optimal power distribution over the active diameter of the photodiode on the one hand, but at the same time minimize beam walk generated by any pointing jitter in the measurement beams. This is essential to avoid the generation of pathlength noise by projection of pointing jitter into the longitudinal signal. Both functions can be realized by a classical pupil relay system, for which a detailed design is presented in Figure 15. Including consideration of manufacturing and alignment tolerances, all three designs achieve a wavefront error of better than $\lambda/10$ rms with only spherical lens surfaces, and are optimized for suppression of residual ghosts. An intermediate image plane is foreseen for installation of a field stop.

The lenses and field stop would be mounted in front of the Quadrant Photodectors within individual, thermally compensated mounts in an optical subassembly such as illustrated in Figure17. Since these subassemblies are installed in a section
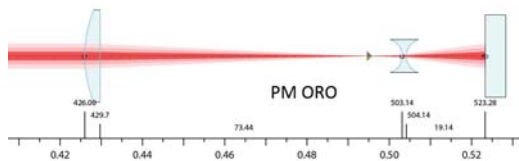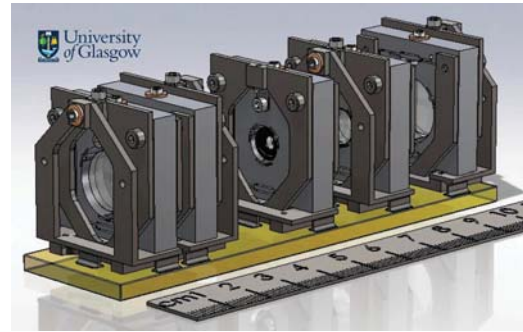
where measurement and reference beam are already recombined, pathlength fluctuations generated within the lenses by thermal fluctuations are suppressed in common mode.

The amount of lenses within the pupil relay systems as well as the space occupied by them on the OB motivated the investigation of alternative optical design approaches for the interferometric imaging. An example relying on the specific properties of Gaussian beams is illustrated in Figure 16, which realizes suppression of beam walk and provision of the appropriate beam diameter with only two commercially available lenses. However, conclusive demonstration of its interferometric imaging performance is depending on experimental test, as is the final validation of the pupil relay imaging approach, both of which are currently pending.

Thermally compensated mounts with lateral fine adjustment capability over monolithically integrated flexures, similar to the ones utilized for the imaging systems, ensure exact centering of the Quadrant Photodiodes within the output plane of the respective imaging system. The QPD mount, depicted in Figure 18, further supports a Polarcor® polarizer and a beam clip in coaxial arrangement, which realizes well-defined beam limitation to the active area of the QPD as well as stray light control.

The QPD beat signals with a bandwidth of 2 - 19 MHz are conditioned for transmission in a front-end electronic placed in very close proximity to the QPD, and enclosed in a dedicated RF housing made from aluminum. The front-end

Fig. 16. Example of an alternative imaging design for the PM ORO, based on only 2 commercially available lenses.

Fig. 18. Photodiode assembly consisting of a precision flexure mount for the Quadrant Photodiode and an RF enclosure for the front-end electronic. An actual prototype of the QPD mount is seen on the right.
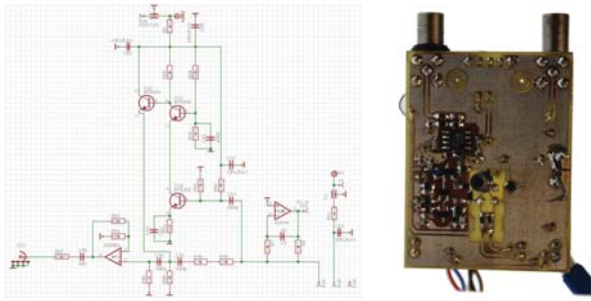
Fig. 19. Circuit layout and two-channel prototype of the QPD front-end electronics.
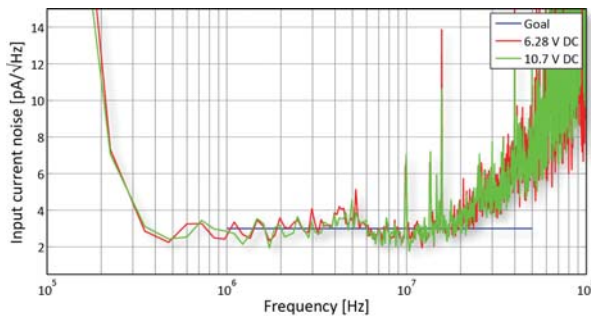

Fig. 20. Measured input current noise of the prototype trans-impedance amplifier at two different reverse voltages. The blue line indicates the design goal of $3\,\mathrm{pA}/\sqrt{\mathrm{Hz}}$

Fig. 21. Measured amplitude and phase response of the prototype transimdepance amplifier front-end.

electronic, shown in Figure 19, provides for each quadrant of the QPD a DC channel with a bandwidth of about $10\,\mathrm{kHz}$ and an AC channel, in which the beat note is processed by a low noise trans-impedance amplifier based on a cascode circuit. In shot noise limited operation, which is relevant in particular for the Science Interferometer, the essential figure of merit characterizing the noise performance of the circuit is the input current noise of the amplifier. If P_{lo} and P_{sig} are the optical power levels of local oscillator and signal beam on the respective quadrant, η_{resp} is the responsivity of the semiconductor, and η_{het} is the heterodyne efficiency, the pathlength measurement noise generated by input current noise of magnitude δI would be

$$\delta L = \frac{\lambda}{2\pi}\sqrt{\frac{\delta I^2}{2\eta_{resp}^2\eta_{het}P_{lo}P_{sig}}}.$$

For the conditions of the Science Interferometer, with a total signal power of approx. $200\,\mathrm{pW}$, this implies that an input current noise of not much more than $3\,\mathrm{pA}/\sqrt{\mathrm{Hz}}$ would be desirable. Despite the presence of some oscillations at higher frequencies, this is basically achieved by the present prototype, as shown in Figure 20. Also the bandwidth has been measured to be compliant with the requirements, see Figure 21.

Only few commercially available quadrant photodiodes were identified to be potentially compatible with the needs of an application on the OB. Figure 22 summarizes the properties of the models taken into closer consideration. Two conflicting requirements drive the selection: a large bandwidth can only be achieved with a low capacitance, but a large active area avoids the need for extreme beam compression and thus eases
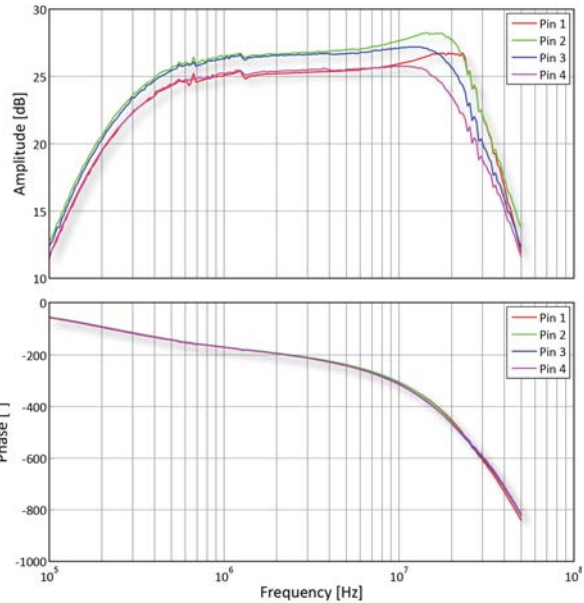
optical design and relaxes alignment tolerances.

The First Sensor QP22-Q appeared to provide the best compromise of these aspects. However, when tested in terms of its spatially resolved response, a hexagonal spot pattern was observed both in the amplitude and the phase signal (Figure 23). This pattern may cause increased coupling of incident beam jitter into the longitudinal signal, and is therefore potentially harmful in the context of interferometry. The pattern matches with features on the back of the silicon die, which are used to contact the diode to its electrode. These feedthroughs are required since the diode has both a relatively thick absorptive layer and a reflective coating on the back of this layer, to enhance its responsivity at infrared wavelengths. The reflective layer is intentionally rough, which in turn causes an increased optical cross-talk close to the edge of each quadrant. Further experiments with the QP22-Q revealed also a much lower bandwidth than expected from the capacitance quoted in the data sheet, which was attributed to
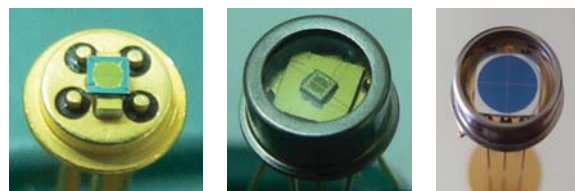
Supplier	OEC	Hamamatsu	First Sensor
Type	GAP 1000Q	G6849-01	QP22-Q
Semiconductor	InGaAs	InGaAs	Enhanced Si
Responsivity	0.68 A/W	~ 0.65 A/W	0.55 A/W
Dark Current	6 nA @ 5 V	0.18 nA @ 5 V	0.8 nA @ 150 V
Capacitance	15 pF @ 5 V	11 pF @ 5 V	3 pF @ 150 V
Active Area	⌀ 1 mm	⌀ 1 mm	⌀ 5.33 mm
Gap Width	20 μm	30 μm	70 μm

Fig. 22. Selection of candidate Quadrant Photodiodes considered for implementation on the OB EBB.
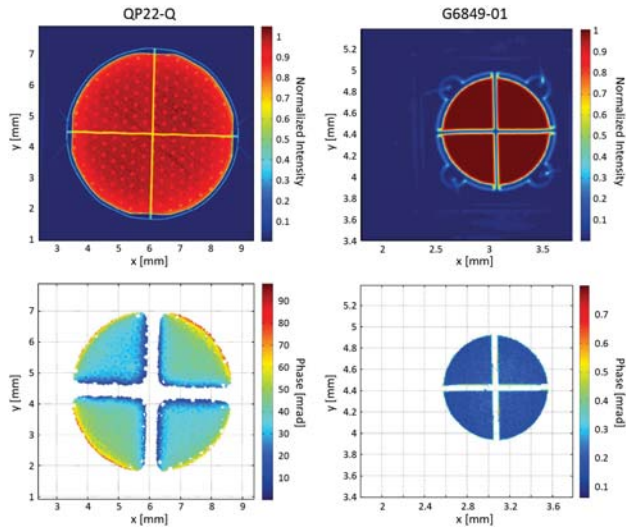
Fig. 23. Spatially resolved response for the QP22-Q and the G6849-01. The measurement was performed by scanning a pencil beam with a spot size of $w_0 = 21\,\mu m$ over the active area. For observation of the phase response, two laser frequencies separated by 10 kHz were generated within the same pencil beam, and their relative phase was referenced to a second, stable photodiode.

photoelectron transport dynamics within the thick absorptive layer. In consequence, only the GAP 1000Q by OEC and the G6849-01 by Hamamatsu presently remain candidate QPDs for the OB EBB. The latter also did not reveal any distinct features in spatially resolved tests (Figure 23).

VII. ACQUISTION CAMERA

The Acquistion Sensor is a camera designed for detection of the RX beam over a field of view of $\pm 200\,\mu rad$, corresponding to wavefront tilts of ± 16 mrad at the internal telescope pupil. This pupil is imaged onto a CCD by the camera optics depicted in Figure 24. Its effective focal length is 160 mm, and it realizes a diffraction limited image with an Airy radius of $35\,\mu m$. The image size is designed to be compatible with the chip size of the selected CCD, the SU320KTS-1.7RT by Goodrich ISR Systems, which has 320×256 pixels at $25\,\mu m$ pitch. It is illustrated in Figure 25.

In order to guarantee a well-controlled handover of the RX beam acquisition to Differential Wavefront Sensing in the Science Interferometer, the Acquisition Sensor has to provide a pointing resolution on the order of $\pm 10\,\mu rad$ at the telescope interface, corresponding to $1.6\,\mu m$ on the CCD, or 0.06 pixels. This is achieved by applying threshold center of gravity centroiding, by which a centroiding accuracy of better than ± 0.01 pixels could be demonstrated with the actual hardware. While this is well within the requirement, the centroiding is subject to pixelization, as shown in Figure 26. The magnitude

Fig. 24. Optical design for the camera transferring wavefront tilt at the internal pupil of the telescope into spot position on the CCD.
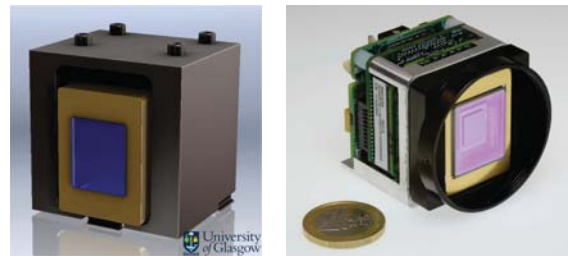

Fig. 25. Opto-mechanical mounting of the CCD (left), and selected CCD sensor (SU320KTS-1.7RT by Goodrich ISR Systems, right).
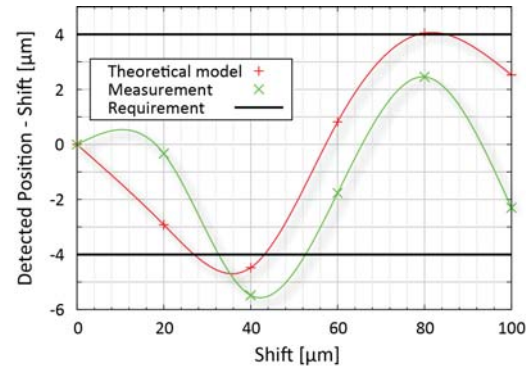

Fig. 26. Measured centroiding performance, showing a periodic error known as pixelization.

of this periodic error is found to be on the order of $\pm 5\,\mu m$, and thus only marginally acceptable. Calibration may potentially be applied for a correction of the effect.

VIII. CONCLUSIONS

In summary, all subsystems required for the realization of the Optical Bench elegant breadboard, designed specifically for the mission scenario of LISA, but covering also functions and performances applicable to NGO, have been fully detailed, procured, and validated in essential aspects. After assembly of the Optical Bench EBB in the next step, further functional and performance testing will validate the Optical Bench metrology concepts on system level. This includes in particular an end-to-end test of the entire metrology chain, including interferometric imaging and photodetector behavior. For this purpose, it is necessary to close the open optical interfaces of the Optical Bench towards the telescope and the Proof Mass. This is accomplished by a dedicated Telescope & Proof Mass Simulator, which also is currently under development [12], together with an extensive suite of further special test equipment [13].

REFERENCES

[1] J. E. Faller, P. L. Bender, J. L. Hall, D. Hils, and M. A. Vincent, "Space Antenna for Gravitational Wave Astronomy". In ESA Colloq. in Kilometric Opt. Arrays in Space, pp. 157-163 (1985).

[2] M. Sallusti, P. Gath, D. Weise, M. Berger, and H. R. Schulte, "LISA System Design Highlights". Class. Quantum Grav. 26, 094015 (2009).

[3] P. F. Gath, D. Weise, H. R. Schulte, and U. Johann, "LISA Mission and System Architectures and Performances". Journal of Physics: Conference Series 154, 012013 (2009).

[4] N. Dunbar, E. Fitzsimons, P. Gath, A. Gianolio, U. Johann, S. Kemble, M. Perreur-Llyod, N. Saks, Ch. Trenkel, P. Weimer, and D. Weise, "Mission, System, and Payload Architecture for the New Gravitational Wave Observatory". 9th Int. LISA Symposium (2012).

[5] E. Morrison, B. J. Meers, D. I. Robertson, and H. Ward, "Experimental demonstration of an automatic alignment system for optical interferometers". Applied Optics 33(22), pp. 5037 (1994).

[6] E. Morrison, B. J. Meers, D. I. Robertson, and H. Ward, "Automatic alignment of optical interferometers". Applied Optics 33(22), pp. 5041 (1994).

[7] D. Weise, P. Marenaci, P. Weimer, M. Berger, H. R. Schulte, P. Gath, and U. Johann, "Opto-Mechanical Architecture of the LISA Instrument". Proceedings of the 7th International Conference on Space Optics, Toulouse (2008).

[8] E. J. Elliffe, J. Bogenstahl, A. Deshpande, J. Hough, C. Killow, S. Reid, D. Robertson, S. Rowan, H. Ward, and G. Cagnoli, "Hydroxide-catalysis bonding for stable optical systems for space". Class. Quantum Grav. 22, S257 (2005).

[9] S. Ressel, M. Gohlke, D. Rauen, T. Schuldt, W. Kronast, U. Mescheder, U. Johann, D. Weise, and C. Braxmaier, "Ultrastable assembly and integration technology for ground- and space-based optical systems". Applied Optics 49(22), pp. 4296 (2010).

[10] L. d'Arcio, J. Bogenstahl, M. Dehne, C. Diekmann, E. D. Fitzsimons, R. Fleddermann, E. Granova, G. Heinzel, H. Hogenhuis, C. J. Killow, M. Perreur-Lloyd, J. Pijnenburg, D. I. Robertson, A. Shoda, A. Sohmer, A. Taylor, M. Tröbs, G. Wanner, H. Ward, and D. Weise, "Optical Bench Development for LISA". Proceedings of the 8th International Conference on Space Optics, Rhodes (2010).

[11] J. Pijnenburg, N. Rijnveld, H. Hogenhuis, "Extremely stable piezo mechanisms for LISA/NGO", Proceedings of the 9th International Conference on Space Optics, Ajaccio (2012).

[12] J. Bogenstahl, L. d'Arcio, M. Tröbs, C. Diekmann, E. D. Fitzsimons, J.-S. Hennig, F. G. Hey, C. J. Killow, M. Lieser, S. Lucarelli, M. Perreur-Lloyd, J. Pijnenburg, D. I. Robertson, H. Ward, D. Weise, G. Heinzel, and K. Danzmann, "Design and construction of a telescope simulator for LISA optical bench testing". Proceedings of the 9th International Conference on Space Optics, Ajaccio (2012).

[13] M. Tröbs, L. d'Arcio, S. Barke, J. Bogenstahl, I. Bykov, M. Dehne, C. Diekmann, E. D. Fitzsimons, R. Fleddermann, O. Gerberding, J.-S. Hennig, F. G. Hey, H. Hogenhuis, C. J. Killow, E. Kochkina, J. Kullmann, M. Lieser, S. Lucarelli, M. Perreur-Lloyd, J. Pijnenburg, D. I. Robertson, A. Shoda, A. Sohmer, A. Taylor, G. Wanner, H. Ward, D. Weise, G. Heinzel, and K. Danzmann, "Testing the LISA optical bench". Proceedings of the 9th International Conference on Space Optics, Ajaccio (2012).